



# Nitroxide Diradical EPR Lineshapes and Spin Relaxation

Joseph P. Y. Kao<sup>1</sup> · Whylder Moore<sup>2</sup> · Lukas B. Woodcock<sup>2</sup> ·  
Nathaniel D. A. Dirda<sup>1</sup> · Eric A. Legenzov<sup>1</sup> · Sandra S. Eaton<sup>2</sup> · Gareth R. Eaton<sup>2</sup>

Received: 26 February 2021 / Revised: 4 June 2021 / Accepted: 9 June 2021 /  
Published online: 30 June 2021

© The Author(s), under exclusive licence to Springer-Verlag GmbH Austria, part of Springer Nature 2021

## Abstract

EPR line shapes in fluid solution and electron spin relaxation times and lineshapes in frozen solution were measured at X-band for two dinitroxides. For dinitroxide **1**, which has two proxyl nitroxides connected by an amide linkage, the fluid solution spectra are in the strong exchange limit ( $J \gg$  nitrogen hyperfine coupling) and the interspin distance in glassy water:glycerol is about 8.8 Å. For dinitroxide **2**, which has two proxyl nitroxides connected by a bridging ethylenediamine and two amide linkages, the fluid solution spectra are characteristic of dynamic exchange between conformations with strong exchange ( $J > 850$  MHz) and conformations with weaker exchange interaction. For **2**, the interspin distance in glassy water:glycerol is about 9.2 Å and  $J > 600$  MHz.  $T_1$  and  $T_m$  for both dinitroxides in 1:1 water:glycerol were measured at 10 to 160 K. Relaxation times are within experimental uncertainty of values for a pyrrolinoxyl monoradical and very similar to values for a nitroxide with a piperidiny ring. These data demonstrate that even for these relatively flexible linkages dipolar interaction with an interspin distance of about 9 Å does not provide an effective spin–lattice relaxation mechanism for dinitroxides in glassy water:glycerol.

## 1 Introduction

The EPR spectra of species containing two nitroxide radicals have fascinated and informed scientists for well over a half century [1], and continue to reward study. Dinitroxides have been designed to report a wide range of properties including dynamics in solution [2], conformational changes of peptides, exchange pathways through bonds and through space, coordination to paramagnetic metal complexes [3], and dipolar interactions. Dinitroxide radicals are being used to maximize

---

✉ Joseph P. Y. Kao  
jkao@som.umaryland.edu

<sup>1</sup> Center for Biomedical Engineering & Technology (BioMET) and Department of Physiology, University of Maryland School of Medicine, 111 Penn Street, Baltimore, MD 21201, USA

<sup>2</sup> Department of Chemistry and Biochemistry, University of Denver, Denver, CO 80210, USA

dynamic nuclear polarization (DNP) [4]. Disulfide-linked dinitroxides can measure *in vivo* physiology via cleavage of the –S–S– bond by reducing agents, predominantly glutathione [5–7]. Proof of principle imaging of tumor redox status by dinitroxides has been achieved [7].

Dipolar interactions are the foundation for the widely used methods of measuring distances in polymers and biomolecular systems, including proteins and nucleic acids [double electron–electron resonance (DEER), pulsed electron double resonance (PELDOR), and double quantum coherence (DQC)] [8, 9]. Experience with the well-separated nitroxide labels used in DEER reveals that the  $T_1$  and  $T_m$  relaxation times are affected by the lattice environment (other paramagnetic species, nearby methyl groups, and deuteration) and not by the effect of one nitroxide on the other [10–12]. Diradicals with interactions strong enough to cause spin–spin splittings in the continuous wave (CW) spectra in solution have shortened  $T_2$  relaxation times that are seen as broadened lines in fluid solution [13, 14]. Relatively few measurements have been made of relaxation times in frozen solution or other rigid lattice.

Data reported previously by Sato et al. [15] showed that for dinitroxides with  $J \gg A_N$  the nitrogen hyperfine interaction ( $A_N$ ) modulation of nitroxide–nitroxide dipolar interactions at distances of 5 to 6 Å enhanced spin–spin ( $T_m$ ) and spin–lattice ( $T_1$ ) relaxation in rigid lattice. However, in a diradical with a relatively rigid azine linkage and interspin distance of 9 Å,  $T_1$  and  $T_m$  were similar to values for a monoradical. Those results left unresolved the question whether relaxation enhancement at a distance as long as 9 Å would be greater if the linker in the diradical were more flexible. In this paper, we report CW lineshape analysis and electron spin relaxation times at temperatures between 10 and 160 K for two dinitroxides with interspin distances of about 9 Å and  $J \gg A_N$ , but with more flexible amide and ethylenediamine linkers.

## 2 Experimental

### 2.1 General

Two nitroxide building blocks were used in this study: 3-carboxy-2,2,5,5-tetramethylpyrrolidin-1-oxyl (3-carboxyproxyl) was obtained from the N. N. Vorozhtsov Novosibirsk Institute of Organic Chemistry, and 3-amino-2,2,5,5-tetramethylpyrrolidin-1-oxyl (3-aminoproxyl) was purchased from ACROS Organics. The coupling reagent, *O*-(benzotriazol-1-yl)-*N,N,N',N'*-tetramethyluronium hexafluorophosphate (HBTU), was from Oakwood Products. Common reagent chemicals and solvents, of ACS grade or better, were purchased from commercial vendors and used without further purification. Silica Gel 60 plates (MilliporeSigma) were used for thin-layer chromatography (TLC). Synthetic products were purified on prepacked silica gel columns on a flash chromatography system (AKROS, Yamazen Science, Inc.). High-resolution mass spectrometry (HRMS) was performed on an electrospray ionization (ESI) instrument (AccuTOF-CS, JEOL) at the Mass Spectrometry Facility in the Department of Chemistry and Biochemistry at the University of Maryland, College

Park. Continuous wave (CW) EPR spectra at room temperature were recorded on a Bruker EMXnano X-band spectrometer. EPR samples were contained in 50- $\mu$ L borosilicate capillary micropipettes (Drummond Scientific Company) whose ends were closed with sealing clay.

## 2.2 Synthesis of Dinitroxides

### 2.2.1 *N*-(2,2,5,5-Tetramethylpyrrolidin-1-oxyl-3-yl)-2,2,5,5-tetramethylpyrrolidin-1-oxyl-3-carboxamide (**1**)

3-Aminoproxyl (90.0 mg, 0.572 mmol), 3-carboxyproxyl (107 mg, 0.572 mmol), and HBTU (217 mg, 0.572 mmol) were weighed into a 20-mL glass reaction vial containing a magnetic stir bar. Dry dimethylacetamide (DMA, stored over 3 Å molecular sieves; 1.5 mL) and diisopropylethylamine (DIPEA; 100  $\mu$ L, 74 mg, 0.572 mmol) were added, causing complete dissolution. The vial was sealed with a silicone septum-cap, purged with dry argon, and sealed with Parafilm. The reaction mixture was stirred overnight (~16 h). The mixture was dried under vacuum to a thick residue, which was partitioned between EtOAc (10 mL) and K-phosphate buffer (8 mL; 1 M, pH 2). The organic phase was washed again with K-phosphate buffer (8 mL), and then with half-saturated NaHCO<sub>3</sub> (8 mL). The EtOAc phase was dried over anhydrous Na<sub>2</sub>SO<sub>4</sub>, filtered, reduced by rotary evaporation, and dried under vacuum. By TLC (2:1 EtOAc:hexane), the crude product showed a predominant component with *R<sub>f</sub>*=0.17. Appropriate fractions from flash chromatography on silica (EtOAc:hexane gradient elution) were pooled and dried to afford pure **1** as a yellow solid (146 mg, 78.4%). HRMS (ESI+): [M+H]<sup>+</sup> C<sub>17</sub>H<sub>32</sub>N<sub>3</sub>O<sub>3</sub> requires 326.2444, found 326.2439.

### 2.2.2 *N,N'*-Bis(2,2,5,5-tetramethylpyrrolidin-1-oxyl-3-carbonyl)ethylenediamine (**2**)

Dinitroxide **2** was prepared using a modified literature procedure [16]. 3-Carboxyproxyl (400 mg, 2.15 mmol) was weighed into a 20-mL glass reaction vial containing a magnetic stir bar; dry benzene (5 mL) and anhydrous pyridine (191  $\mu$ L, 0.187 g, 2.36 mmol) were then added. The vial was sealed with a silicone septum-cap, chilled in an ice-water bath, and purged with dry argon. Addition of SOCl<sub>2</sub> (219  $\mu$ L, 0.358 g, 3.00 mmol) in two aliquots by syringe caused the yellow reaction mixture to turn orange, with rapid formation of flocculent precipitate. The mixture was quickly warmed to room temperature and stirring continued for a further 65 min. The solids were separated from the solution by passage through a PTFE syringe filter; several small volumes of benzene were used to rinse residual reaction solution from the solids. The combined filtrate was concentrated in a fresh 20-mL vial by rotary evaporation and dried under vacuum to give the crude acid chloride as a brown oil, which was used immediately in the next step. The brown oil was dissolved in dry CHCl<sub>3</sub> (stored over 3 Å molecular sieves; 5 mL), and to the solution was added DIPEA (412  $\mu$ L, 0.305 g, 2.36 mmol). The mixture was chilled in an ice-water bath and ethylenediamine (71.8  $\mu$ L, 64.5 mg,

1.07 mmol) was added in one portion, whereupon precipitates formed immediately. The vial was sealed with a silicone septum-cap, sealed with Parafilm, and stirring was continued overnight (~20 h). The mixture was diluted with  $\text{CHCl}_3$  (10 mL), first extracted with K-phosphate buffer ( $2 \times 8$  mL; 1 M, pH 2), and then with half-saturated  $\text{NaHCO}_3$  ( $2 \times 8$  mL). The organic phase was dried over anhydrous  $\text{Na}_2\text{SO}_4$ , filtered, concentrated by rotary evaporation and dried under vacuum to an amber foam. The crude product showed one predominant component by TLC (9:1 EtOAc:MeOH) with  $R_f=0.23$ . Flash chromatography on silica (EtOAc:MeOH gradient elution) gave pure fractions and some fractions containing a trace of faster running impurity. When reduced to dryness, the impure fractions amounted to 73 mg of mass. The pure fractions gave pure **2** as a very viscous yellow oil, which gradually crystallized over several days (209 mg, 49.1%). HRMS (ESI+):  $[\text{M}+\text{H}]^+$   $\text{C}_{20}\text{H}_{37}\text{N}_4\text{O}_4$  requires 397.2815, found 397.2815.

### 2.3 EPR Spectroscopy

CW spectra at temperatures above ambient were measured on a Bruker EMX X-band spectrometer, using an HSQE resonator, at incident microwave powers in the linear response region. The 0.2 mM samples in 1:1 water:ethanol were contained in a thin Teflon tube, placed in a 4-mm o.d. quartz tube open at both ends. Nitrogen gas was passed over the sample to remove  $\text{O}_2$  from the solution. The  $\text{N}_2$  gas was heated to achieve the sample temperature, which was measured with a thermocouple above the resonator. The sample temperature probably was higher than the recorded temperature due to the vertical thermal gradient.

Relaxation times of nitroxides and dinitroxides in glassy 1:1 water:glycerol are sufficiently long that low microwave power and modulation must be used to record undistorted spectra. Much better signal-to-noise can be achieved by 2-pulse field-swept echo detection than by CW. First derivative spectra were calculated from the echo-detected absorption spectra by pseudomodulation [17] in Matlab.

Time-domain spectra were measured using a Bruker E580 pulsed EPR spectrometer using 0.2 mM solutions in 1:1 water:glycerol. Two-pulse spin echo and three-pulse inversion recovery experiments were performed with  $\pi/2$ -pulse lengths of 40 ns. The ER4118X-MD5-W1 resonator was in a CF935 cryostat. Temperature was controlled with a Bruker/ColdEdge Stinger closed-cycle helium system for temperatures between 4 and 70 K, or with  $\text{N}_2$  gas from liquid  $\text{N}_2$  in a dewar via an Oxford Instruments transfer line for temperatures between 80 and 260 K. Temperature at the resonator was measured with a Lakeshore Cernox sensor.

Most of the 3-pulse inversion recovery measures of  $T_1$  and the 2-pulse spin echo decay measures of the phase memory time,  $T_m$ , were not simple exponentials. The reported values for  $T_m$  were obtained by fitting the experimental data with a stretched exponential. Values of  $T_1$  are the longer time of a fit with a

double exponential. We assume, but have not proven, that the shorter time is due to spectral diffusion.

## 2.4 Simulations of EPR Spectra

Fluid solution spectra were simulated with a previously described MATLAB program developed for use with EasySpin [2, 18]. The  $g_{\text{iso}}=2.0058$  and  $A_{\text{N}}=43.7$  MHz for both **1** and **2** were selected to fit the spectra and are in good agreement with prior reports for pyrrolidine nitroxides [19]. Simulations of spectra for **1** are based on a single value of  $J$  and were not improved by adding a contribution from a second component with a different value of  $J$ . Simulations of spectra for **2** are based on interconversion of two conformations with substantially different values of  $J$ . Rigid-lattice spectra were simulated with custom software originally written for spin-coupled metal–nitroxide spectra [20]. Values of  $J$  were assumed to be  $\gg A_{\text{N}}$ . Decreasing  $J$  did not improve the simulations. The value of interspin distance was adjusted to match the extent of the spectra. The angles that define the relative orientations are shown in Figure 1 of Ref. [20]. The simulations are very sensitive to the orientation of the interspin vector relative to the z-axes of both nitroxides and relatively insensitive to rotation around the z-axis, which is not surprising given the relatively small anisotropy of the nitroxide parameters in the x, y plane.  $\varepsilon$  is the angle between the electron–electron interspin vector and the z-axis of one nitroxide, and  $\eta$  is the angle that is defined by the projection of the interspin vector on the x, y plane of that nitroxide. The angles used to calculate the simulation for **1** were  $\varepsilon=75^\circ$  and  $\eta=60^\circ$ . The simulation parameters for **2** were  $\varepsilon=65^\circ$  and  $\eta=25^\circ$ . The angle between the z-axes of the two nitroxides is  $\alpha_1$  and the other two Euler angles are  $\alpha_2$  and  $\alpha_3$ . For nitroxides **1** and **2** the values of  $\alpha_1$ ,  $\alpha_2$ , and  $\alpha_3$  that were used in the simulations were  $150^\circ$ ,  $75^\circ$ , and  $0^\circ$  and  $110^\circ$ ,  $10^\circ$ , and  $0^\circ$ , respectively. The nitroxide parameters were  $g_x=2.0089$ ,  $g_y=2.0066$ ,  $g_z=2.0025$  and  $A_x=A_y=15$  MHz,  $A_z=105$  MHz [19].

The temperature dependence of  $1/T_1$  was modeled as the sum of contributions from the direct process (or other processes with similar dependence on the reciprocal of temperature), the Raman process, and a local mode [21].

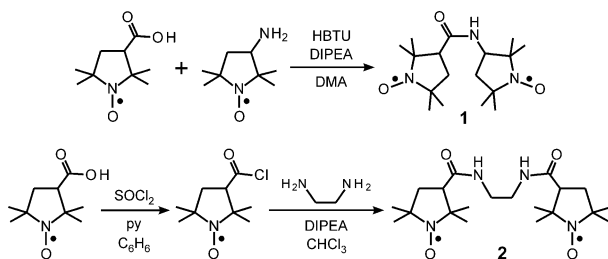


**Fig. 1** Synthesis scheme for dinitroxides **1** and **2**. Abbreviations: HBTU = 1*H*-1-[bis(dimethylamino)methylene]-benzotriazolium-3-oxide hexafluorophosphate; DIPEA, diisopropylethylamine; DMA, *N,N*-dimethylacetamide; py, pyridine

### 3 Results and Discussion

Dinitroxide **1**, consisting of two proxyls connected by a single amide linkage, was prepared in good yield through a condensation reaction, as shown in the first scheme in Fig. 1. However, when the same reaction conditions were used in an attempt to synthesize dinitroxide **2**, the yield was very poor (~15%). We, therefore, modified the procedure of Ehman and colleagues, who first reported the synthesis of **2** [16]. As shown in the second scheme in Fig. 1, 3-carboxyproxyl was converted to the acid chloride, which was immediately used in reaction with ethylenediamine to give **2** in reasonable yield.

#### 3.1 Fluid Solution Spectra

CW spectra of **1** in 1:1 water:ethanol (Fig. 2) exhibit the 5-line 1:2:3:2:1 relative intensity pattern that is characteristic of dinitroxides with  $J \gg A_N$  [2, 22]. The simulated spectra were calculated for a single species with  $J = 1000$  MHz. Increasing  $J$  had no impact on the simulation. Multiple conformations may be present that are interconverting rapidly on the EPR timescale. The lines are sufficiently broad that removal of  $O_2$  by purging with  $N_2$  had little impact on the linewidths. Increasing temperature from 21 to 55 °C caused the linewidths to decrease by about a factor of 2. Since the viscosity of 1:1 water:ethanol decreases by about a factor of two over this temperature interval [23], the

**Fig. 2** Spectra as a function of temperature for 0.2 mM dinitroxide **1** in 1:1 water:ethanol, purged with  $N_2$  gas (solid lines). Simulations (dashed lines in overlays with experimental data) used  $J = 1000$  MHz and Gaussian  $\Delta B_{pp}$  linewidths that decreased with temperature: 0.26 mT at 21 °C, 0.19 mT at 30 °C, and 0.13 mT at 55 °C. To highlight the changes in linewidths, the simulations are overlaid in the lower panel using the same colors at each temperature as in the upper panels

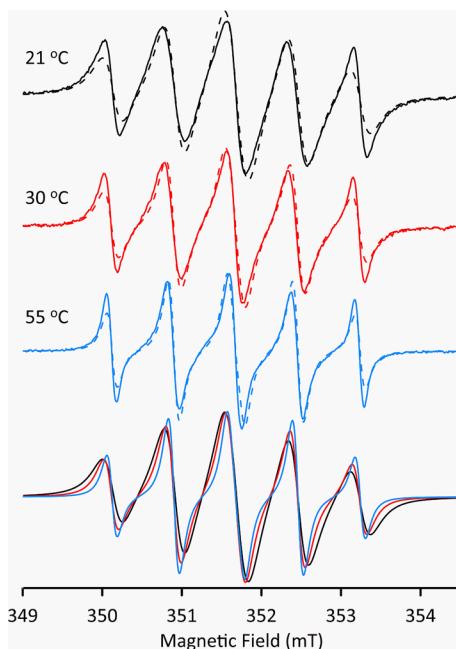
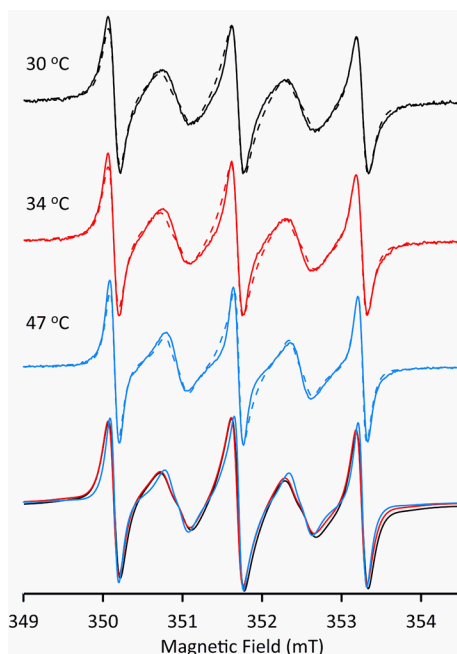


**Fig. 3** Spectra as a function of temperature for 0.2 mM dinitroxide **2** in 1:1 water:ethanol, purged with N<sub>2</sub> gas (solid lines). Simulations (dashed lines in overlays with experimental data) used two conformations with  $J = 1000$  MHz and 20 MHz, respectively. The ratio of populations of the conformations with the larger and smaller values of  $J$  increased from 2.1 to 2.2 to 2.7 at 21, 34, and 47 °C, respectively. Gaussian  $\Delta B_{pp}$  linewidths decreased from 0.15 to 0.14 to 0.11 mT at 30, 34, and 47 °C, respectively. The rate of conversion from the conformation with smaller  $J$  to the one with larger  $J$  was  $7 \times 10^6$  s<sup>-1</sup>. To highlight the changes in lineshapes the simulations are overlaid in the lower panel using the same colors as each temperature as in the upper panels



decrease in linewidths with increasing temperature is attributed to faster tumbling that more effectively averages  $g$  and  $A_N$  anisotropy and the anisotropy of the dipolar interaction between the unpaired electrons.

CW spectra of **2** in 1:1 water:ethanol (Fig. 3) exhibit the ‘alternating linewidth’ effect that is characteristic of systems with dynamic processes occurring on the timescale of the EPR experiment [24]. For this and many other dinitroxides, the dynamic process is interpreted as interconversion of conformations that differ substantially in the value of  $J$  [2]. The lowest field and highest field lines of the 5-line pattern arise from molecules with  $m_1 = +1$  or  $m_1 = -1$  for both nitroxide nitrogens and have resonance positions that are independent of the value of  $J$ . The central line has contributions from molecules with  $m_1 = 0$  for both nitrogens as well as partially averaged contributions from molecules with one nitrogen  $m_1 = -1$  and one  $m_1 = +1$ . The lines at intermediate positions are partially averaged contributions from molecules with one  $m_1 = -1$  and one  $m_1 = 0$  or one  $m_1 = 0$  and one  $m_1 = 1$ . The positions of these intermediate lines are strongly dependent on the values of  $J$  and the rates of interconversion of conformations with different values of  $J$ . The simulations shown in Fig. 3 are based on two conformations with  $J = 1000$  and 20 MHz. These values probably represent ensembles of relatively rapidly interconverting conformations. Simulations were not improved by the addition of a third conformation with an intermediate value of  $J$ . The population of the conformation with the larger value of  $J$  increased with increasing temperature, which has been observed in other flexible diradicals [22].

### 3.2 Rigid Lattice Spectra

Rigid-lattice spectra for **1** and **2** in 1:1 glassy water:glycerol at 80 K are shown in Fig. 4. The values of  $J$  are  $> 850$  or  $> 650$  MHz, respectively, which are  $\gg A_N$ . Decreasing  $J$  resulted in poorer agreement between simulation and experiment. Increasing  $J$  had no observable impact on the calculated spectra. Simulations of the rigid lattice spectra were obtained with  $r = 8.8 \pm 0.3$  Å for **1** and  $r = 9.2 \pm 0.4$  Å for **2**. The spectral extents are strongly dependent on the interspin distance,  $r$ , so there is relatively little uncertainty in  $r$ . The values  $r$  for **1** and **2** are consistent with conformations calculated in the gas phase with the molecular dynamics program WebMO. Because of the flexibility of the linkers, there is a variety of conformations with similar energies. There is substantially greater uncertainty in the angular parameters that define the conformations of the diradicals than in the values of  $r$ . The splittings in the rigid lattice spectra depend on the relative orientations of the hyperfine axes, which are strongly dependent on conformations. The

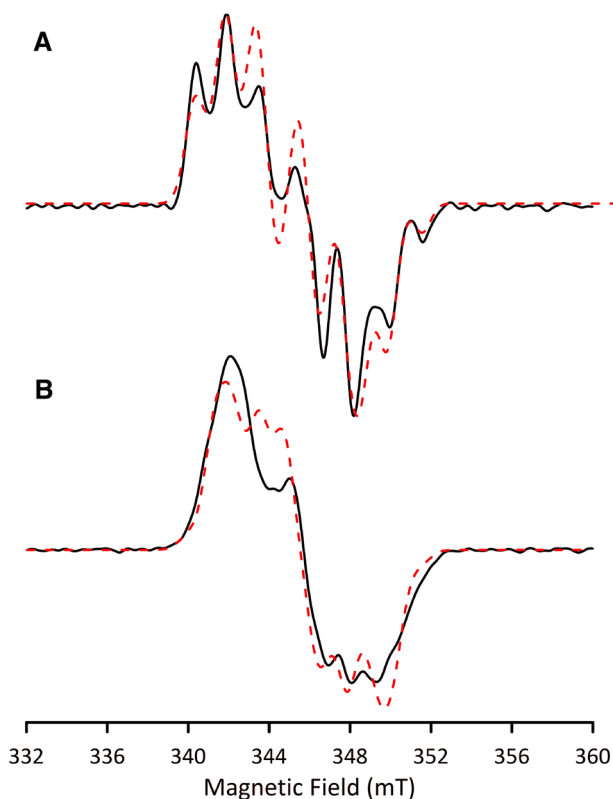


**Fig. 4** First derivatives of X-band two-pulse field-swept echo-detected spectra for **A 1** and **B 2** in 1:1 water:glycerol at 80 K. Simulations (red dashed lines) were obtained with the parameters given in the text



imperfect agreement between experimental data and simulations in Fig. 4 may be due to overlapping spectra from different conformations.

### 3.3 Relaxation Times

Electron spin relaxation times for dinitroxides **1** and **2** in 1:1 water glycerol at 10 to 160 K are shown in Fig. 5. Relaxation times are compared with values for the monoradical MTSL, which contains a five-membered pyrroline ring similar to that in **1** and **2**, and the values for tempone, which contains a six-membered piperidine ring. Below about 70 K  $T_m$  is similar for the two dinitroxides, MTSL, and tempone, and values are approximately independent of temperature. In this temperature range  $T_m$  is dominated by nuclear spin diffusion of solvent protons [11]. Above about 70 K  $1/T_m$  increases similarly for the four samples and is attributed to the rotation of the gem-dimethyl groups at rates that are comparable to the anisotropy of the proton-electron couplings that are averaged by the rotation [25]. The temperature-dependent values of  $T_1$  for the two dinitroxides, MTSL, and tempone are very similar and could be modeled as the sum of contributions from a direct process (or other processes

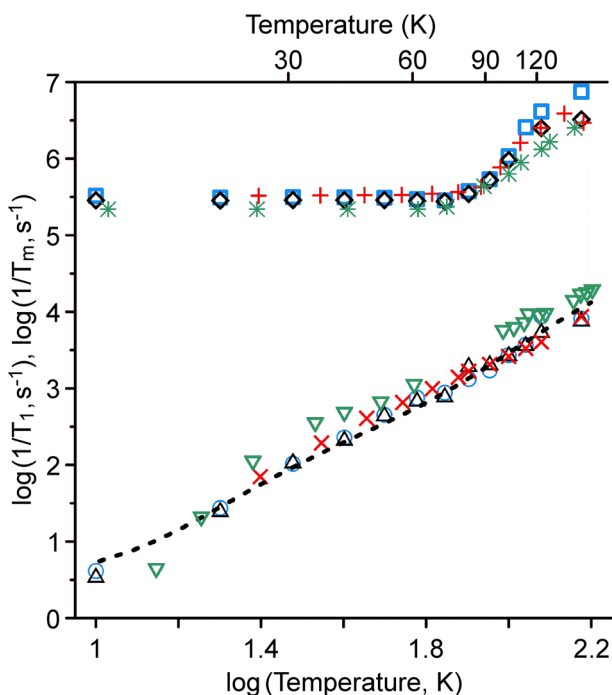
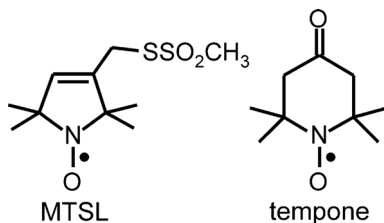


**Fig. 5** Temperature dependence in 1:1 water:glycerol of  $1/T_1$  for **1** (blue circles), **2** (black triangles), MTSL (red  $\times$ ), and tempone (green inverted triangles), and  $1/T_m$  for **1** (blue squares), **2** (black diamonds), MTSL (red  $+$ ), and tempone (green  $*$ ). The black dashed line is a model based on contributions from the direct process (or other processes with similar temperature dependence), Raman process, and local mode

with similar temperature dependence), Raman process, and a local mode. These processes are typical for organic radicals [21].



### 3.4 Comparison with Prior Results

Sato et al. [15] measured  $T_1$  and  $T_m$  of structurally related mono-, di-, and tetradicals, with interspin distances of 5 to 9 Å and  $J$  values several orders of magnitude larger than for diradicals **1** and **2**. The diradicals with interspin distances of 5–6 Å had shorter  $T_m$  relaxation time than the monoradical of the same molecular frame, and both relaxed much faster than the monoradical Frémy's salt (peroxylamine disulfonate). In the temperature range above ca. 70 K, methyl rotation dominated  $T_m$ . The data in Sato et al. [15] demonstrated that modulation of dipolar interaction between spins 5–6 Å apart is a major contributor to both  $1/T_1$  and  $1/T_m$ . The  $1/T_1$  relaxation rate of the tetradical was more than an order of magnitude faster than that of the related diradical, and three orders of magnitude faster than that of the monoradicals. In glycerol, a rigid diradical with large  $J$  had the same relaxation rate at X-band and Q-band. A local mode dominated the relaxation above about 80 K. The relaxation enhancement was greater for the tetradicals than for the diradicals. The motions involved in Raman and local mode relaxation enhance relaxation of di- and tetradicals. Above the softening point modulation of the spin–spin interaction becomes a very important relaxation mechanism. When motion is large enough to result in dynamic variation in exchange interactions, relaxation becomes very efficient.

However, Sato et al. showed that an azo-linked diradical with spin–spin distance ca. 9 Å had the same  $T_1$  relaxation times as a related monoradical. The absence of an impact of spin–spin interaction on the relaxation rates for the azo-linked diradical could be the result of the very rigid linker. In **1** and **2**, the linker is more flexible than the azo linkage. The new data for **1** and **2** confirm that modulation of dipolar interactions at distances of about 9 Å is not an effective electron spin relaxation mechanism, even for dinitroxides with relatively flexible linkers.

The extensive literature reporting the use of dinitroxide radicals to enhance dynamic nuclear polarization in NMR includes direct measurements of electron spin relaxation [26–29]. Many of the relaxation measurements were made on ca. 10 mM solutions, as commonly used in DNP experiments. The very large effect of spin concentration is illustrated by the data for 0.2 mM and 16 mM solutions from [27]. Relaxation times in high-concentration samples exhibited non-exponential  $T_1$  recoveries and  $T_m$  decays. When approximated as a double-exponential, the shorter

component was interpreted as a spectral diffusion time. Some 0.1 mM solutions were measured at 9 GHz and 97 K [29]. One set of measurements on a dinitroxide showed that there was no change in  $T_1$  at 100 K from 9.5 to 260 GHz [28]. The inversion recovery time and spin echo decay time at 100 K in 16 mM tetrachloroethane solutions, measured at 94 GHz, was roughly proportional to molecular weight [27], consistent with the observations of Sato et al. [12].

**Acknowledgements** This work was supported in part by National Institutes of Health (R01 GM124310-01 SSE), the University of Denver, and the Nanobiology Research Fund of the University of Maryland Baltimore Foundation.

## References

1. E.G. Rozantsev, *Free Nitroxyl Radicals* (Plenum Press, New York, 1970)
2. S.S. Eaton, L.B. Woodcock, G.R. Eaton, *Conc. Magn. Reson. A* (2018). <https://doi.org/10.1002/cmr.a.21246>
3. B.M. Sawant, G.R. Eaton, S.S. Eaton, *J. Magn. Reson.* **45**, 162–169 (1981)
4. D.J. Kubicki, G. Casano, M. Schwarzwald, S. Abel, C. Sauvee, K. Ganesan, M. Yulikov, A.J. Rossini, G. Jeschke, C. Coperet, A. Lesage, P. Tordo, O. Ouari, L. Emsley, *Chem. Sci.* **7**, 550–558 (2016)
5. G.I. Roshchupkina, A.A. Bobko, A. Bratasz, V.A. Reznikov, P. Kuppussamy, V.V. Khrantsov, *Free Rad. Biol Med.* **45**, 312–320 (2008)
6. E.A. Legenzov, S. Muralidharan, L.B. Woodcock, G.R. Eaton, S.S. Eaton, G.M. Rosen, J.P.Y. Kao, *Bioconj. Chem.* **27**, 2923–2930 (2016)
7. B. Epel, S.V. Sundramoorthy, M. Krzykowska-Serda, M.C. Maggio, M. Tseytlin, G.R. Eaton, S.S. Eaton, G.M. Rosen, J.P.Y. Kao, H.J. Halpern, *J. Magn. Reson.* **276**, 31–36 (2017)
8. G. Jeschke, *Annu. Rev. Phys. Chem.* **63**, 419–446 (2012)
9. Y.D. Tsvetkov, M.K. Bowman, Y.A. Grishin, *Pulsed Electron-Electron Double Resonance* (Springer International Publishing, Switzerland, 2019)
10. S.S. Eaton, G.R. Eaton, in *Distance Measurements in Biological Systems by EPR*. ed. by L.J. Berliner, G.R. Eaton, S.S. Eaton (Springer US, Boston, 2000), pp. 29–154
11. A.N.A. Zecevic, G.R. Eaton, S.S. Eaton, M. Lindgren, *Mol. Phys.* **95**(6), 1255–1263 (1998)
12. H. Sato, V. Kathirvelu, A. Fielding, J.P. Blinco, A.S. Micallef, S.E. Bottle, S.S. Eaton, G.R. Eaton, *Mol. Phys.* **105**(15–16), 2137–2151 (2007)
13. G.R. Luckhurst, *Mol. Phys.* **10**(6), 543–550 (1966)
14. S.S. Eaton, L.B. Woodcock, G.R. Eaton, *Concepts Magn. Reson. Part A* **47A**(2), e21426 (2018)
15. H. Sato, V. Kathirvelu, G. Spagnol, S. Rajca, S.S. Eaton, G.R. Eaton, *J. Phys. Chem. B.* **112**, 2818–2828 (2008)
16. R.L. Ehman, R.C. Brasch, M.T. McNamara, U.L.F. Eriksson, G. Sosnovsky, J. Luksz, S.W. Li, *Invest. Radiol.* **21**(2), 125–131 (1986)
17. J.S. Hyde, A. Jesmanowicz, J.J. Ratke, W.E. Antholine, *J. Magn. Reson.* **96**(1), 1–13 (1992)
18. S. Stoll, A. Schweiger, *J. Magn. Reson.* **178**, 42–55 (2006)
19. J.R. Biller, H. Elajaili, V. Meyer, G.M. Rosen, S.S. Eaton, G.R. Eaton, *J. Magn. Reson.* **236**, 47–56 (2013)
20. S.S. Eaton, K.M. More, B.M. Sawant, P.M. Boymel, G.R. Eaton, *J. Magn. Reson.* **52**(3), 435–449 (1983)
21. S.S. Eaton, G.R. Eaton, in *EPR Spectroscopy: Fundamentals and Methods*. ed. by D. Goldfarb, S. Stoll (John Wiley & Sons Ltd, Chichester, 2018), pp. 175–192
22. V.N. Parmon, A.I. Kokorin, G.M. Zhidomirov, *Zh. Strukt. Khim.* **18**, 104–147 (1977). (in English translation)
23. I.S. Khattab, F. Bandarkar, M.A.A. Fakhree, A. Jouyban, *Korean J. Chem. Eng.* **29**, 812–817 (2012)
24. G.R. Luckhurst, *Mol. Phys.* **10**, 543–550 (1966)
25. A. Rajca, V. Kathirvelu, S.K. Roy, M. Pink, S. Rajca, S. Sarkar, S.S. Eaton, G.R. Eaton, *Chem. Eur. J.* **16**, 5778–5782 (2010)

26. A. Zagdoun, G. Casano, O. Ouari, G. Lapadula, A.J. Rossini, M. Lelli, M. Baffert, D. Gajan, L. Veyre, W.E. Maas, M. Rosay, R.T. Weber, C. Thieuleux, C. Coperet, A. Lesage, P. Tordo, L. Emsley, *J. Am. Chem. Soc.* **134**, 2284–2291 (2012)
27. A. Zagdoun, G. Casano, O. Ouari, M. Schwarzwaldler, A.J. Rossini, F. Aussenac, M. Yulikov, G. Jeschke, C. Coperet, A. Lesage, P. Tordo, L. Emsley, *J. Am. Chem. Soc.* **135**, 12790–12797 (2013)
28. C. Sauvee, G. Casano, S. Abel, A. Rockenbauer, D. Akhmetzyanov, H. Karoui, D. Siri, F. Aussenac, W. Maas, R.T. Weber, T. Prisner, M. Rosay, P. Tordo, O. Ouari, *Chem. Eur. J* **22**, 5598–5606 (2016)
29. C. Sauvee, M. Rosay, G. Casano, F. Aussenac, R.T. Weber, O. Ouari, P. Tordo, *Angew. Chem. Int. Ed.* **52**, 10858–10861 (2013)

**Publisher's Note** Springer Nature remains neutral with regard to jurisdictional claims in published maps and institutional affiliations.